(Preprint) AAS 20-500

DATA ASSOCIATION EXPERIMENTS USING REAL RADAR DATA

Benedikt Reihs[*], Alessandro Vananti[†], Thomas Schildknecht[‡], Jan A. Siminski[§] and Tim Flohrer [¶]

The monitoring of the space object population, especially the space debris population, is an important aspect of space safety to enable the safe operation of near-Earth space missions. One of the main components of such a space surveillance system is the maintenance of a space object database, commonly called catalogue, which can be used for e.g. conjunction assessment and re-entry casualty risk estimation. The build-up and maintenance of such a database requires the continuous, automated processing of observations to create new database entries and maintain the accuracy of existing ones.

To support the initialisation of new objects into the database, it is advantageous to use multiple passes of an object to have a more reliable orbit compared to that from a single pass. To identify such associated passes, previous work by the authors include the development of a method to test whether two measured passes, called tracklets, originate from the same object in which case they are called to be correlated. This method was tested on simulated measurement data and showed promising results. The present paper uses real radar measurements from two LeoLabs radars in the United States to further validate and characterise the method, mainly for objects in low earth orbit. The first tests confirm that the method's initial orbit determination which includes the secular J_2-perturbation works for the maximum time span of circa 24 days between two tracklets. The correlation which also requires the selection of the correct number of revolutions between the two tracklets works reliably for 1-2 days before the selection of a wrong number of revolutions increases, which is also dependent on the geometry of the two passes. Further experiments test the sensitivity of the method to e.g. distributed stations, atmospheric drag and manoeuvres. Finally, different approaches to a cold-start of a database are tested using either least squares orbit determination or a graph network for object confirmation. Overall results show that the developed methods works well with real radar data and can contribute to the build-up of a space object database.

INTRODUCTION

With the constant increase of the space debris population , see (Reference 1), space surveillance becomes crucial to safe operations of satellites. One of the common tasks of a space surveillance system is the creation of a database, commonly called catalogue, of resident space objects (RSOs) with their corresponding orbit and possibly further information. Different sensors can be used to contribute to such a catalogue. While telescopes are usually used to observe high-altitude objects

[*]PhD student, Astronomical Institute University of Bern (AIUB), Sidlerstrasse 5, 3012 Bern, Switzerland.
[†]Research Associate, Astronomical Institute University of Bern (AIUB), Sidlerstrasse 5, 3012 Bern, Switzerland.
[‡]Professor, Astronomical Institute University of Bern (AIUB), Sidlerstrasse 5, 3012 Bern, Switzerland.
[§]Space Debris Engineer, ESA/ESOC, Robert-Bosch-Str 5, 64293 Darmstadt, Germany.
[¶]Senior Space Debris Monitoring Analyst, ESA/ESOC, Robert-Bosch-Str 5, 64293 Darmstadt, Germany.

close to the geostationary orbit (GEO), the low earth orbit (LEO) is mainly observed by radar. The upcoming upgrade of the US American fence radar will lead to detections of even more objects than today, see (Reference 2), which also becomes a challenge for the data processing. Current developments in the field of radar space surveillance in Europe include the German GESTRA, the EISCAT_3D in Scandinavia, although this is not a dedicated space surveillance sensor, and the Spanish S3T (References 3-5). There is also an emerging trend of commercial operators offering measurement data. In the domain of radar measurements, LeoLabs* is currently operating three radars, two in the United States and one in New Zealand. The data from the US radars is the data source for the present paper.

This work analyses the association of tracklets to each other. A tracklet is defined as a sequence of detections from a single pass of an object at a specific station. For the build-up of a catalogue or if a tracklet cannot be associated to a catalogue object, it is necessary to create a new catalogue object. This might be possible via an initial orbit determination (IOD) on the single tracklet if it is long enough and thus contains sufficient information. To have more confidence in a new catalogue object, it is beneficial to have two or even more tracklets from the same object. If two tracklets can be positively associated to come from the same object, they are called to be correlated. One possible approach for this correlation is to use the orbit from the single tracklet IOD and propagate it together with its covariance to the epoch of another tracklet. Examples for this approach can be found in, e.g. (References 6 and 7). If the tracklets become shorter, these approaches lose their reliability as the IOD becomes less accurate. One possibility to treat this problem is the use of multitarget filters for both IOD and association, see e.g. (References 8 and 9). Another popular approach, which is also the basis for the method used in this paper is the use of attributables, introduced in (Reference 10), which includes fitting a polynomial over the raw measurements to generate a virtual measurement with less uncertainty than the single measurements. This fitting approach has been analysed for optical measurements by (Reference 11) and optical attributables have been used successfully in methods for the correlation of short-arc optical tracklets, e.g. (References 12-14). Radar attributables have been defined in (Reference 15) and they have been used for correlation in, e.g. (References 16-18). Furthermore, (Reference 19) contains an analysis of the fitting of attributables depending on the tracklet lengths and its influence on the correlation performance. The following paper analyses the correlation performance of the method by (Reference 18) using real measurements from the LeoLabs radars.

CORRELATION METHOD

One radar detection can consist of up to four observables: the range ρ, the range-rate $\dot{\rho}$, the azimuth az and the elevation el. The attributables are derived by fitting a polynomial function to the raw measurements. After the appropriate transformations, the attributable contains the three-dimensional inertial position of the detected object and the measured range-rate, both at the same epoch. Combining two attributables results in two positions with their corresponding range-rates. These two positions can be used to determine an initial orbit using the approach described in (Reference 18). This correlation method consists of two steps. First, an initial orbit determination is performed, which includes the secular effects of the J_2-perturbation and derives an orbit for all possible numbers of revolutions between the two attributables. The main feature of the IOD is to rotate the position of the later detected attributable around the Earth rotation axis to counteract the rotation of the orbital plane between the two detections. Apart from the secular J_2-perturbation, the propa-

*https://www.leolabs.space/

gation in the IOD is Keplerian and does not consider drag or other perturbations. For each derived orbit, it can be calculated what measurement of the range-rate would have been expected from such an orbit at the two epochs. The difference between these expected range-rates and the measured ones from the attributable are scaled by their uncertainty to calculate the Mahalanobis distance M_{d}, see (Reference 20) . Under the assumption of normally distributed measurement errors, the Mahalanobis distance theoretically follows a χ-distribution, which allows it to be used for probabilistic gating decisions. The minimum of all Mahalanobis distances from the different numbers of revolutions can be chosen as the most likely trajectory between the tracklets. If this distance is below a defined threshold value $M_{\mathrm{d,\,thresh}}$, the correlation is accepted and the two tracklets are assumed to originate from the same object.

Focussing only on the minimum of the Mahalanobis distances can lead to the selection of a wrong number of revolutions for the initial orbit. To mitigate this problem, a post-processing procedure was introduced in (Reference 19), which considers the fact that the attributable contains only one position and not all detections of the tracklet. To use all detections, the residuals for both the angles and the range are derived from the calculated initial orbit. Those residuals are tested for correlated errors among them because if the orbit matches the tracklet, the residuals should at least approximately follow a zero mean normal distribution. This test procedure is described in more details in (Reference 19) and will be referred to in the following as *residuals post-processing* (RPP). This additional test allows it to use more information than just the Mahalanobis distance for the correlation decision with regard to the selection of the most probable number of revolutions between the two detections.

For the analysis of the results, there are different possible outcomes of the correlation attempt. A *false positive* (FP) correlation is an identified association of tracklets from two different objects as opposed to a *true positive* (TP) which is a correlation of two tracklets from the same object and thus the desired outcome. The third category is a *false negative* (FN), which indicates a true correlation that has not been identified as such. Due to the multiple solutions from the IOD, it is also possible to have a true positive with a wrong number of revolutions between the tracklets, thus a *wrong orbit* (TPWO).

LEOLABS RADAR DATA

LeoLabs currently operates three radars: the Poker Flat Incoherent Scatter Radar (PFISR) in Alaska (US), the Midland Space Radar (MSR) in Texas (US) and, the most recent addition, the Kiwi Space Radar (KSR) in New Zealand. The data set used for this work contains radar data from the PFISR and the MSR in the time period from 27 March 2019 to 22 April 2019. The detected objects are mainly in LEO. In total there are more than 10 000 different objects in the data set. The number of passes is 301 287 in total, 232 111 for PFISR and 69 176 for MSR. The two radars have different numbers of passes due to their different sensitivity and design. MSR is a one-dimensional phased array radar with a fence-like field of regard (FoR) along one direction. This also leads to much shorter passes compared to PFISR. PFISR is a two-dimensional phased array radar with a star-shaped FoR and thus can cover a larger part of an object's pass above the horizon. For more information on the radars, see e.g. (References 21 and 22). The radar data also contains an association of the detections to the object IDs, which makes it possible to check the identified correlations for their correctness by assuming these given object-tracklet associations as the ground truth.

The data consists of scheduled tracking arcs which for PIFSR may include several short mea-

surement bursts separated by possibly tens of seconds long gaps during the pass. This leads to a distribution of measurement points which is much different than that of a survey radar, like the one considered in (Reference 19). Because the data is mainly intended for the update of already catalogued objects, the radar data focuses on the range and range-rate information, which are the two precisely measurable observables for a radar. However, as explained in the previous section, the IOD requires positions and thus also the angular information is required. The data itself contains only the pointing direction of the radar beam without any further quantification of the uncertainty or beamwidth, which makes the derivation of the attributables more challenging.

The attributables are fitted according to (Reference 19) but the angular observables, i.e. azimuth and elevation, need special treatment. Artificial Gaussian white noise is added to the angular measurements to consider the uncertainties during the least squares fit through the observations. For PFISR, there may be large gaps without a measurement during one pass as explained earlier. To avoid problems with the fit due to these gaps, the measurements from a single pass are split if there is a gap of more than 15 seconds. After this split, only the subset of the measurements with most detections is used for the attributable fitting. This reduces the length of the fitted arc significantly compared to the arc length measured from first to last detection of the entire pass, but it is necessary in order to improve the fitting. The attributable is fitted and defined in the geocentric Attributable Optimised System (AOS), see (Reference 19). This coordinate system is designed to overlay with the orbital plane and provide relatively little variation over an entire pass, even for longer ones and those passing through zenith.

However, this approach also makes it more difficult to estimate the uncertainties from the fit, see (Reference 19). Instead, the errors are estimated from fixed error assumptions for the observables and then transformed into the inertial frame of the positions used in the IOD. Additionally, it has to be considered that real measurement data contains outliers and mis-tagged observations, which makes it also necessary to detect fitted attributables with bad data points in order to remove them.

After the fitting, there are 207 377 attributables for PFISR and 59 924 for MSR. Those contain in total more than 3.5 million true correlations between them, which shows that the data set is well suited for the following association experiments.

For the following experiments, the RPP as described previously is only used for the PFISR data because the MSR's fence-like field of regard makes it difficult to estimate a trend in the angular motion from the pass. In case of PFISR, the entire tracklet is used for the RPP, which also includes parts that may have been ignored for the attributable fit due to gaps between the detections. Also, only full passes with a length of at least four seconds are considered for the RPP, otherwise there is not enough information in the pass to make a decision.

In the following, there are further subgroups of the data set based on the orbital regime. The category *low LEO* refers to the semi-major axis $a \leq 6878$ km, *medium LEO* to 6878 km $\leq a \leq 7278$ km and *high LEO* to 7278 km $\leq a \leq 7578$ km. For all LEO objects there is the condition for the eccentricity $e \leq 0.1$.

TRUE POSITIVE CORRELATION RESULTS

As a first proof-of-concept and to further investigate the attributable-based correlation, the initial experiments in this section test only known true positive correlations, i.e. between tracklets which are known to originate from the same object. This is done in order to quantify the association performance for different scenarios and confirm that the association is possible with the present

data set.

Initial Orbit Determination

Selecting the correct number of revolutions between the two passes is a crucial step in the initial orbit determination and correlation. In order to test the robustness of the perturbed initial orbit determination, some experiments have been performed in which the known true number of revolutions has been used to get only the correct solution. This IOD mode is used to test if it is possible to derive the correct orbit with the developed method, which is a prerequisite for performing the data association and it also gives the maximum achievable correlation performance with this method.

This IOD mode has been performed for the three LEO regimes using tracklets measured with PFISR. Figure 1 shows the resulting percentage of false negatives, i.e. failed initial orbit determinations, over the number of revolutions between the respective tracklets for the medium LEO case, which is representative of all three LEO regimes. The total percentage of FN is 3.11%, without a visible trend for an increasing number of revolutions. The periodic peaks are mainly due to the observation geometry, because if two tracklets are separated by a multiple of a sidereal day and measured at the same station again, the two detections are very close to each other, if they are projected on the orbit. In combination with the nodal precession of the orbital plane, the two measurements are in an inertial frame at similar latitudes but with a shift in longitude which makes it more difficult to find a first orbit to start the J_2-correction, see (Reference 18).

The closer the two measurements are to each other in inertial space, also after the J_2-rotation, the larger is the influence of errors in the attributable's position, especially for estimating the orbital plane. This also leads to the second restriction of the performance, which are bad attributable fits. Although the obvious errors have been filtered but there are still some attributables left in the data set which have an error from the truth that is larger than the assumed uncertainty. However, Figure 1 shows that it is possible to have successful IODs for up to 350 revolutions between the detections, which is equivalent to around 24 days for this orbital regime.

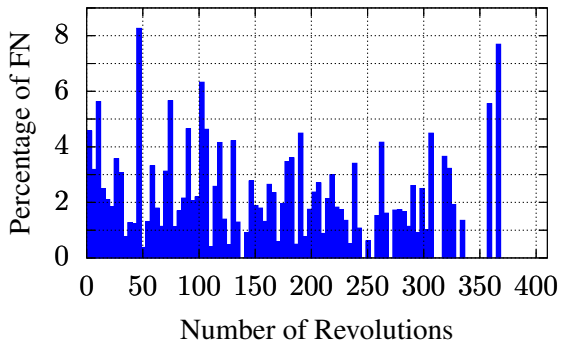

Figure 1: Percentage of false negatives for the initial orbit determination from PFISR measurements.

Correlation Results

The following experiments in this subsection test all true correlations for a given subset of the data, which includes both the association test as well as the selection of the number of revolutions

from the acceptable solutions. As mentioned previously, the RPP is only applied for PFISR, while for the MSR the lowest Mahalanobis distance is always chosen as a solution. For a better presentation of the results, there is a further separation of the correlations into those which have less than three days, less than 100 revolutions and more than three days between the paired tracklets. The cases with less than three days are probably most interesting for the creation of a new catalogue object, whereas the correlations over longer time spans are mainly a test of the method's robustness. Because the computational demand of the correlation increases with the time between the tracklets due to an increased number of possible orbits between them, the tests for less than three days use 10 000 tracklets and those for more than three days use 2 000 tracklets. As a correlation threshold, $M_{\mathrm{d}} < 10$ is used to maximise the identifications.

PFISR

The results of the experiments are given in Figures 2-4 for the medium LEO case as an example, the other two cases have similar results. Considering the false negatives on the right hand side of the plots, the pattern of the peaks due to observations which are multiples of one day apart was already shown and explained for the results of the IOD. The increased number of FN compared to the IOD mode is mainly due to the rejection of the correct solution in the RPP or the failure of an additional check regarding the range-rate differences, which considers that these differences are scaled by their uncertainty to calculate the Mahalanobis distance. Here, another filter has been added which rejects all correlations where the sum of the absolute values of the two range-rate differences is larger than 150 m/s. This is done in order to reject correlations with very large covariances due to their observation geometry. If the covariance reaches a size where a difference of more than 150 m/s is still scaled to $M_{\mathrm{d}} < 10$, nearly anything could be correlated from this pair and to avoid false positives these associations are also rejected.

Considering the percentage of solutions with a wrong orbit, a steady increase with the number of revolutions reaching up to 35% at 100 revolution is observed which finally converges at a maximum of approximately 70%. Focussing on the correlations within 1-2 days, there are usually 5% to 10% of TPWO. It should also be considered that the selection of a wrong orbit does not mean that the correct orbit has not been found but that it was not the selected solution, which will be discussed in in the context of the catalogue build-up using the graph network. Over longer times, there seems to be a pattern in the peaks of the TPWO, but this will be discussed in the following using the MSR data.

MSR

The experiments are again shown for the medium LEO as a representative example in Figures 5-7. The percentage of false negatives is slightly higher than those for the PFISR. Concerning the solutions with a wrong orbit, the dependency on the time between the detections is much stronger than for PFISR because MSR is at a lower latitude. Thus if an object is detected on different segments of its orbit, those detections can be further apart than for the PFISR station which always samples the orbit at northern polar latitudes. The larger spatial separation between the two detections improves the estimation of the orbit and reduces the sensitivity to uncertainties in the measurements. It also helps to select the correct solution concerning the number of revolutions because the range-rates at the two epochs are more representative of the entire orbit. The value of the TPWO for MSR is approximately 80% at the peaks and thus slightly higher than the one for PFISR but between the peaks it reaches much lower levels. It should also be remembered that there is no RPP for the MSR to select the correct number of revolutions.

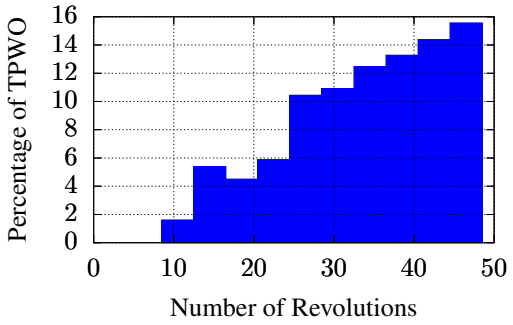

(a) Wrong Orbit

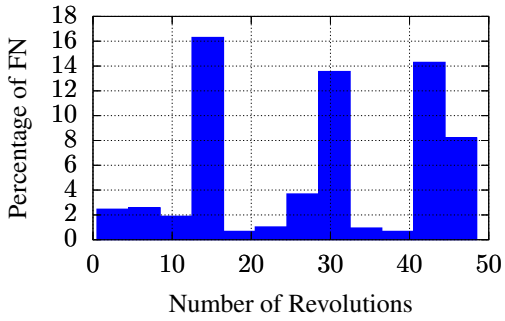

(b) False Negative

Figure 2: Correlation results using PFISR data (medium LEO) for less than three days between the detections.

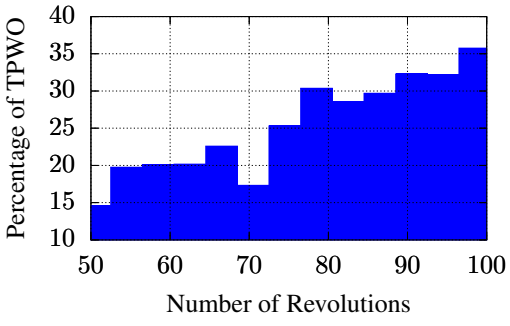

(a) Wrong Orbit

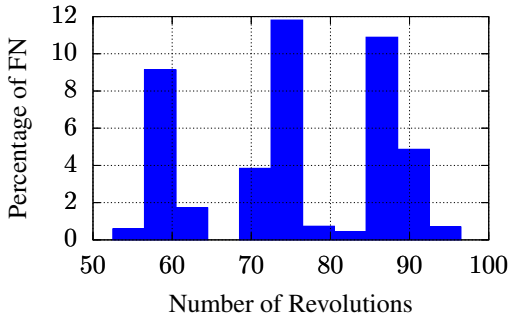

(b) False Negative

Figure 3: Correlation results using PFISR data (medium LEO) for up to 100 revolutions between the detections.

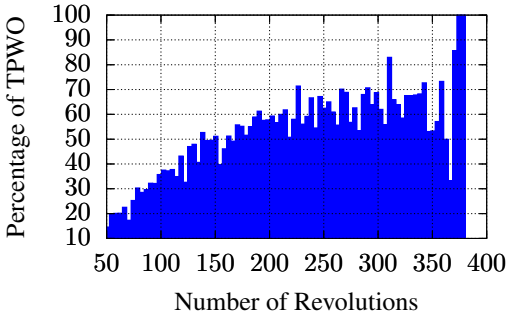

(a) Wrong Orbit

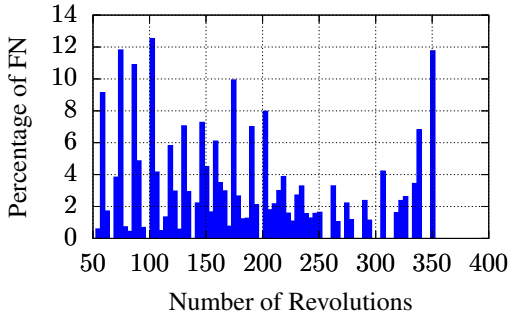

(b) False Negative

Figure 4: Correlation results using PFISR data (medium LEO) for more than three days between the detections.

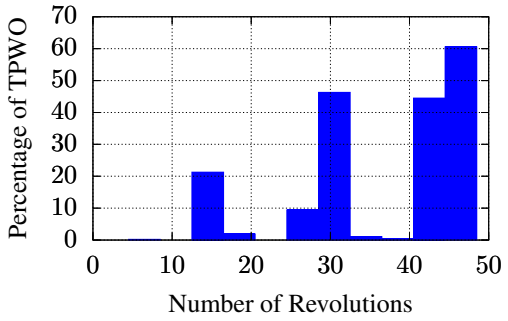

(a) Wrong Orbit

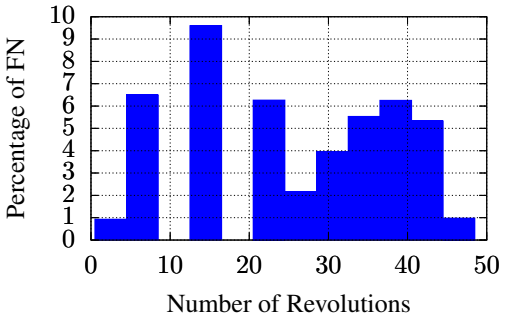

(b) False Negative

Figure 5: Correlation results using MSR data (medium LEO) for less than three days between the detections.

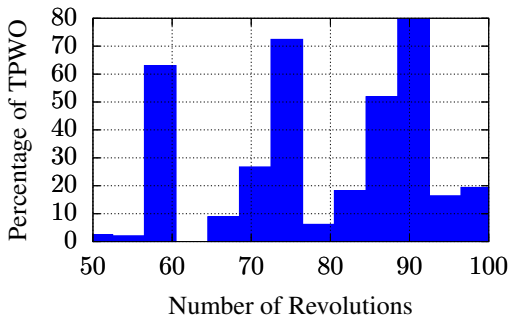

(a) Wrong Orbit

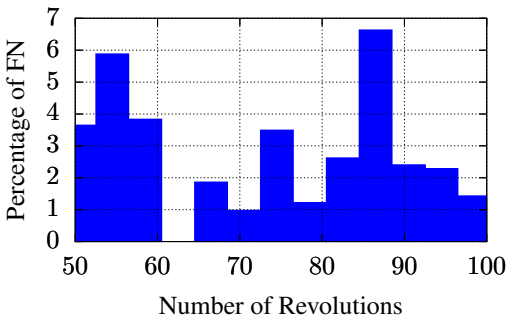

(b) False Negative

Figure 6: Correlation results using MSR data (medium LEO) for up to 100 revolutions between the detections.

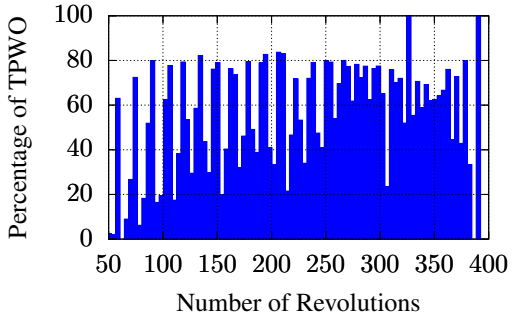

(a) Wrong Orbit

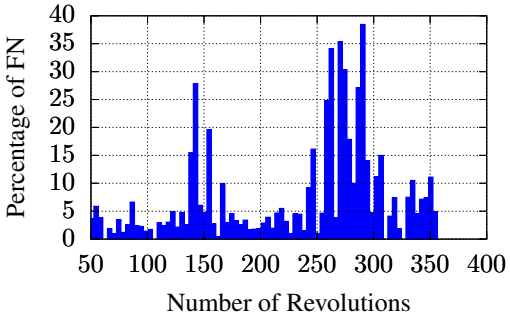

(b) False Negative

Figure 7: Correlation results using MSR data (medium LEO) for more than three days between the detections.

M_d-Distribution

The calculated Mahalanobis distances for the correlations should theoretically follow a χ-distribution with two degrees of freedom, here named $\chi(2)$. Figure 8 shows the relative frequency of the true positive correlations' Mahalanobis distances compared to the theoretical $\chi(2)$-distribution using the medium LEO MSR data from the previous section. It is clearly visible that the resulting distribution does not match the expected one. The J_2-perturbed propagation for the initial orbit determination is only bias-free for a complete revolution, otherwise the short-periodic perturbations lead to discrepancies between the estimated mean motion and the perturbed motion. To confirm this assumption, Figure 9 includes only correlations which are less than one day apart for objects on polar orbits ($80° < i < 100°$) and splits them into those with and without complete revolutions. It is visible that the one with the complete revolutions matches the theoretical distribution sufficiently considering the artificial estimation of the uncertainty. Additionally, the $\chi(2)$-distribution requires normally distributed errors which can probably not be guaranteed with real measurement data and the further non-linearities in the orbit determination process.

Figure 8: Relative frequency of Mahalanobis distances for MSR (medium LEO) compared to the theoretical $\chi(2)$-distribution.

As an additional visualisation, Figure 10 shows the biases in the semi-major axes which result from the bias in the perturbed mean motion over the number of revolutions. These values are derived by comparing the orbit from the correlation with a mean reference orbit from TLE [*]. Those correlations with complete revolutions at $N_{\text{rev}} = [14, 15, 29, 30, 44, 45]$ have normally distributed values around zero mean, whereas the incomplete revolutions show positive or negative biases of the mean depending on the path between the detections. One corresponds to the short path via the north and the other to the long path via the south. The positive and negative biases reduce for an increasing number of revolutions, because the final incomplete revolution becomes less influential. Their absolute mean values are roughly equal for a similar number of revolutions, because they should combine to zero for a complete revolution.

[*] `https://www.space-track.org`

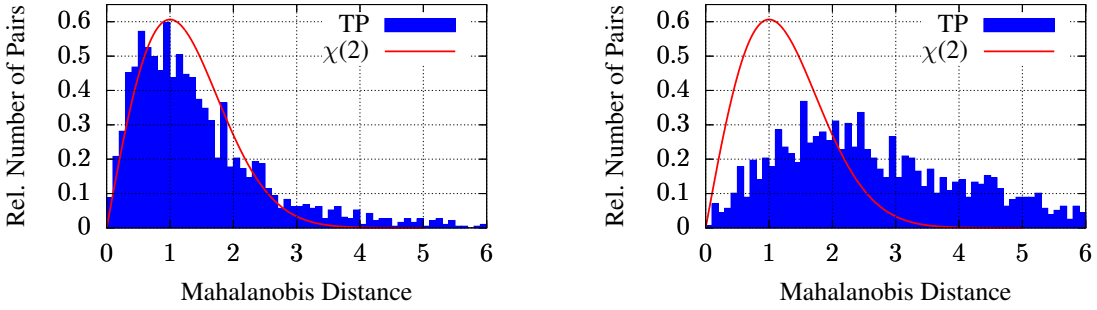

(a) Complete revolutions

(b) Incomplete revolutions

Figure 9: Relative frequency of Mahalanobis distances for MSR (medium LEO, polar orbits, max. one day apart) compared to the theoretical $\chi(2)$-distribution.

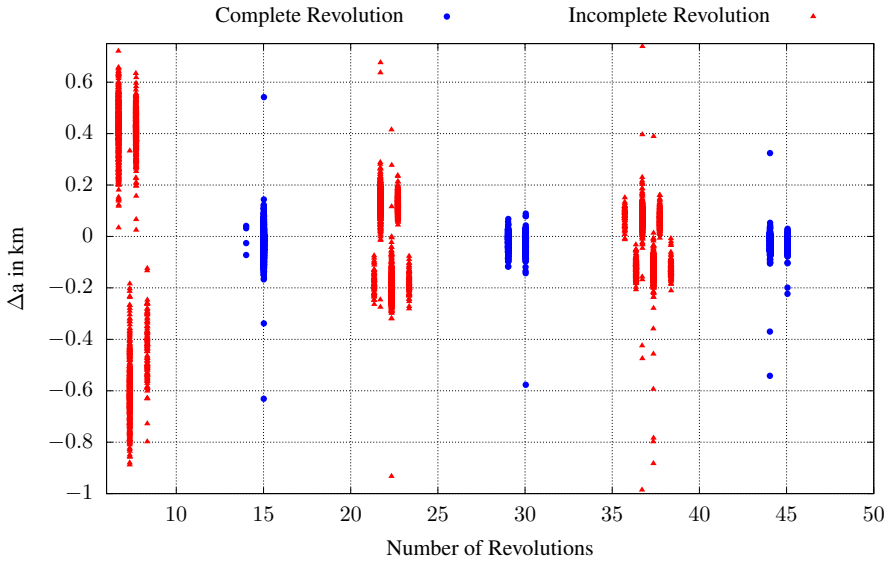

Figure 10: The relation between the number of revolutions (complete and incomplete) and the bias in the semi-major axis for objects on polar orbits (MSR, medium LEO).

Mixed Stations

As a next step, the correlation is attempted with tracklets from different sensors, i.e. one from PFISR and one from MSR. Firstly, the cases for the direct short trajectory between the two stations, i.e. the ones measured at both stations within 10-15 minutes, are considered. The Mahalanobis distances for these correlations are shown in Figure 11a and it is visible that these distances are highly biased and shifted towards larger values. Again this is due to the short-periodic perturbations, which cannot be compensated by further revolutions. This also leads to a large uncertainty on the semi-major axis, see Figure 11b, if the computed semi-major axes are compared to the corresponding reference values.

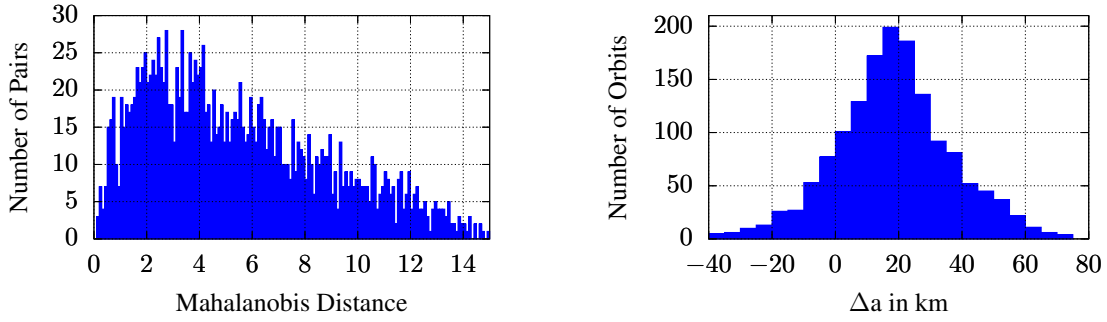

(a) M_{d}-distribution

(b) Estimation error semi-major axis

Figure 11: Correlation results for MSR-PFISR direct short trajectories.

For the remaining correlations, the results are shown in Figures 12-14 using the medium LEO orbits. Considering the FN correlations, the combined case is better than both the MSR and PFISR individually due to the guarantee not to have two measurements very close to each other in inertial space because of the latitudinal separation of the stations. Considering the true positives with wrong orbits, the results should be compared to those of MSR because also the mixed stations case is not using the RPP to select the number of revolutions but only the minimum Mahalanobis distance. This shows that the peaks of TPWO are smaller than those of MSR-only, although the percentages between the peaks are higher now. Because the two stations are still relatively close to each other, the periodic changes in the wrong orbits are visible although less pronounced than for MSR-only.

Influence of Drag

The propagation in the initial orbit determination does not consider drag (Reference 18). In order to show the effect of this limitation, six Microsat-R debris objects resulting from the Indian ASAT test with quickly decaying orbits have been selected from the PFISR data set. These objects are initially at perigee altitudes of 270 km - 340 km and their respective semi-major axes decrease by 10 km - 70 km during the observation campaign. They all re-enter in the following months and thus this is an extreme case of drag-affected orbits. Figure 15 depicts the percentage of false negatives for the IOD of these objects. There is once again a clear pattern showing more FN for detections which are on the same segment of the orbit. This is because an unconsidered change in the orbital altitude is especially difficult to handle for the IOD if the measurements are very close in inertial space. As the most extreme example, consider two detections at exactly the same location on the orbit, but the second detection is lower in altitude due to drag. This makes it impossible to derive an

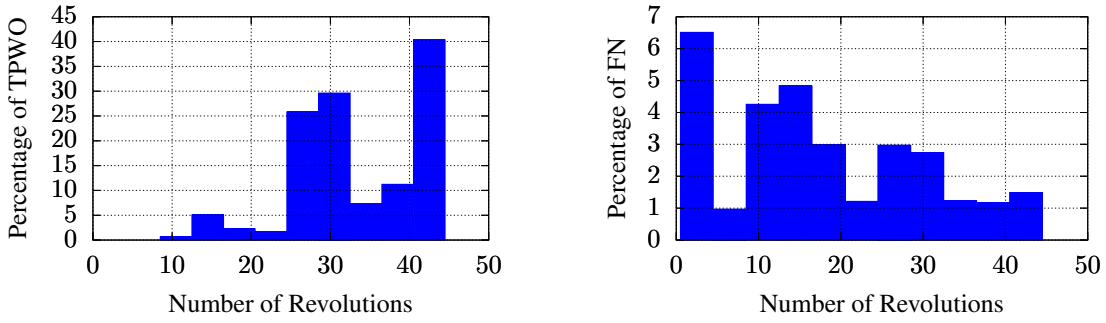

(a) Wrong Orbit (b) False Negative

Figure 12: Correlation results using mixed data (medium LEO) for less than three days between the detections.

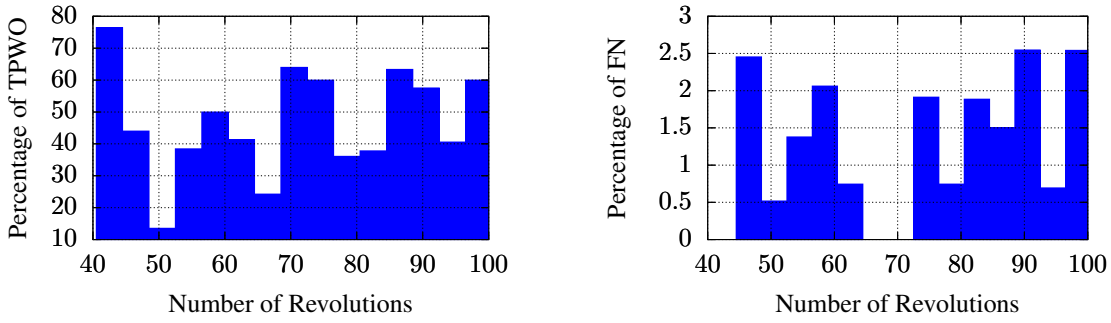

(a) Wrong Orbit (b) False Negative

Figure 13: Correlation results using mixed data (medium LEO) for up to 100 revolutions between the detections.

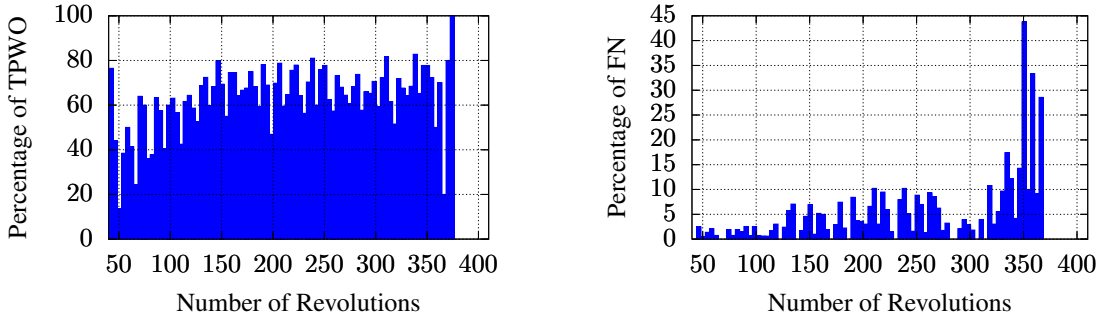

(a) Wrong Orbit (b) False Negative

Figure 14: Correlation results using mixed data (medium LEO) for more than three days between the detections.

orbit around Earth from the two points without considering drag. Due to this effect, drag-affected orbits can be handled better if the measurements are further apart in inertial space, although their semi-major axis and eccentricity may still be estimated imprecisely.

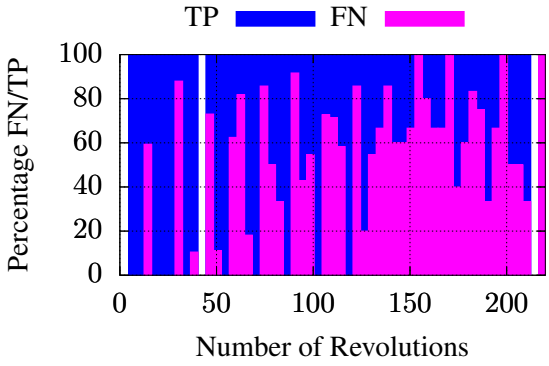

Figure 15: Resulting true positive and false negative IODs using PFISR data of highly drag-affected debris objects.

Influence of Manoeuvres

For the following test, it is analysed how the correlation works in the presence of manoeuvring operational satellites. The ESA missions Sentinel-1A and Aeolus are selected as both perform 5-6 manoeuvres of different types during the campaign. Aeolus performs an orbit raising manoeuvre with a velocity increase in along-track direction of $\Delta v \approx 10 \frac{\text{cm}}{\text{s}}$ every week. Sentinel-1A has one manoeuvre of that size during the considered time frame and some additional smaller manoeuvres.

The IOD mode is used to check whether it is still possible to derive the correct orbit. The results are shown in Figure 16. It is visible that the majority of the initial orbits can be derived. Also analysing the correlations regarding their epoch and comparing them to the manoeuvre epochs does not lead to further insights. Thus it can be concluded that the operational manoeuvres of these satellites are probably too small to have an impact on the initial orbit determination, especially with regards to the other uncertainties in the process.

CATALOGUE BUILD-UP PROCESS

The experiments up to now included only testing the known true correlations. In order to test the build-up of a catalogue, the identification of the true correlations is an important step. Two approaches will be shown in the following. The first one has been described in (Reference 19) and uses an additional least squares orbit determination on the full tracklet with a threshold for the residuals. The second one creates a graph network from all the correlations including the information on the orbit. This approach is based on the internal consistency of the correlations among each other. The following experiments test all correlations from the used subset of the data, thus it is now also possible to have false positive associations.

Least Squares Orbit Determination

This processing approach adds a final least squares orbit determination using all observations from the passes and the orbit from the correlation as an initial solution. To increase the robustness

of this orbit determination, it includes both the Levenberg-Marquardt algorithm as well as a line search along the current step. Outlying measurements are detected and removed by comparing the individual residuals to the mean and standard deviation of the entire set of residuals. A measurement is discarded, if its residual value is more than three standard deviations away from the mean. The angular measurements are used with a low weighting to support convergence, but the orbit determination mainly relies on range and range-rate. The angles are corrupted with additional Gaussian white noise before using them for the orbit determination, because the provided tracking angles are not real measurements and thus do not contain a measurement uncertainty which was explained in the context of the data set.

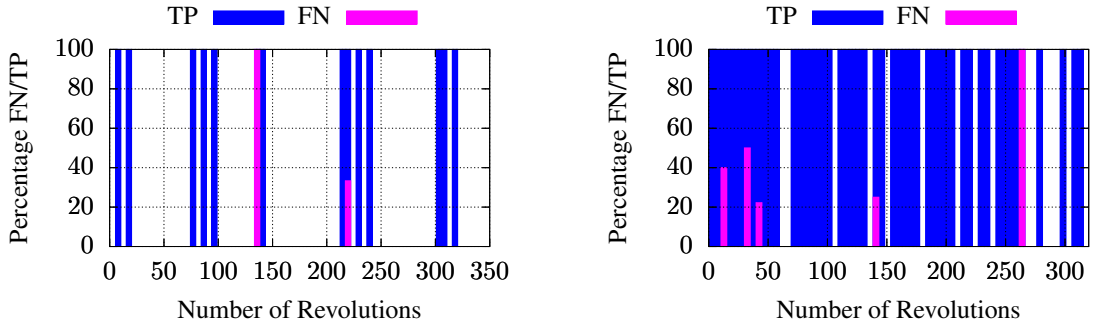

(a) Aeolus

(b) Sentinel-1A

Figure 16: Resulting true positive and false negative IODs using PFISR data of manoeuvring operational ESA satellites.

If the mean μ and standard deviation σ of the residuals over both tracklets of the converged orbit are smaller than the thresholds given in Table 1, the orbit is accepted and the correlation is confirmed. All of the thresholds have to be met, which has proven to be a useful decision criterion. The residuals of the angles are included with a relatively large margin because it helps to remove false positives. These thresholds are certainly not universal, but depend on the radar system. The decision on the threshold values is also an optimisation procedure, because it has to be decided between the number of acceptable false positives and false negatives. In case of a cataloguing approach with additional steps after the least squares, it may be an option to allow more false positives in order to have less false negatives and assume that the cataloguing conditions afterwards filter the false positives. From the results of the previous experiments the threshold to accept a correlation after the first step and process it further is set to $M_{\text{d, thresh}} = 5$.

Table 1: Maximum values of the residuals to accept a least squares fit.

Parameter	μ_{thresh}	σ_{thresh}
Range /m	10	20
Doppler / m/s	5	20
Azimuth / rad	0.015	0.025
Elevation / rad	0.01	0.02

To simulate the regular work of such a cataloguing system, the experiments are performed for one

batch of 24 hours of PFISR data, which gives enough true correlations while keeping the overall processing demand acceptable. There is no assumption of an existing background catalogue which could be used to correlate the observations directly with known objects. Thus, this experiments simulates a cold start of a catalogue.

Single Day - All Tracklets

Using all tracklets measured by PFISR between April 1, 12 UTC and April 2, 12 UTC, circa 8.9 million correlations from 4 216 tracklets have been checked. Only 933 of these correlations are true ones. The results are summarised in Figure 17a. It includes the numbers of true positive, false positive and false negative correlations before and after the additional least squares as well as the number of correlations which were not tested with the least squares because one of the two tracklets was shorter than 4 s. The plot shows that there are approximately 7 500 identified correlations before the least squares with circa 90% false positives. This does not include the correlations which are excluded from the RPP and least squares because of their length. The false negative correlations are those with $M_\mathrm{d} > 5$ or a failed IOD. After the least squares the percentage of false positives has decreased to approximately 16%, while also 84 true positives do not meet the thresholds of the least squares. Subtracting the correlations which are excluded from the least squares, approximately 80% of correlations in the data set have been found.

For the interpretation of these numbers it has to be considered that the measured passes are not optimised for the initial creation of catalogue objects, thus the considered passes might be relatively short. The combination of only two passes is already relatively little information but if these passes are short, then the information content and thus the chance to distinguish confidently between true and false positives becomes less. For example, the majority of accepted false positive correlations has at least one tracklet which is shorter than 15 s. False positive correlations from longer tracklets are also due to the high latitude of PFISR which means that even a hypothetical, non-existent orbit is only sampled around the most northern parts. A better distribution of the measurements could constrain this hypothetical orbit more and possibly lead to the detection of its inconsistency with the measurements. The MSR is not used for this type of experiment because the tracklets are presumably too short to allow a confident initial orbit from two passes.

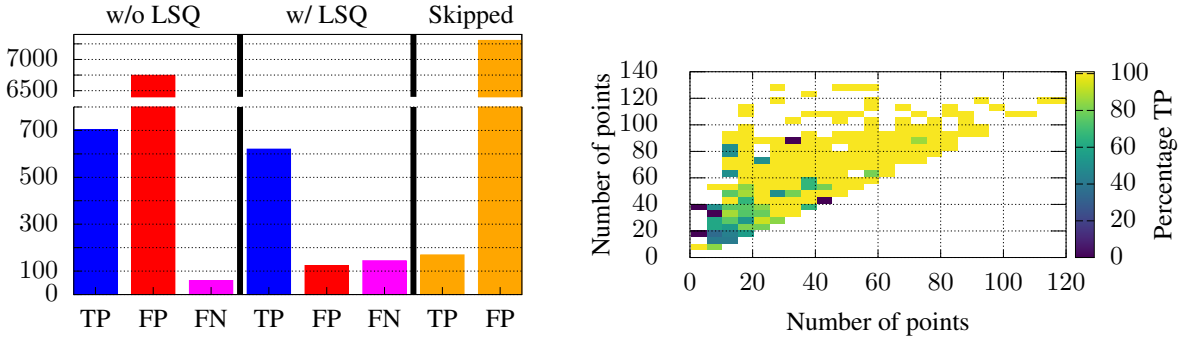

(a) Distributions after different steps

(b) TP depending on number of detections

Figure 17: Correlation results using all PFISR detections within 24 hours.

It also has to be considered that the radar is operating by creating various short tracking arcs, thus the length of the overall pass is not necessarily proportional to the overall data points acquired as it would be for a survey radar. To investigate the influence on the number of data points, Figure 17b

depicts the percentage of true positive correlations within the accepted solutions over the number of data points in the considered passes. It is visible that the majority of false positive correlations have at least one pass with less than 20 detections. Considering the false positives with more than 20 detections in both passes, these are mainly resulting from objects in the Russian communication constellation at $74°$-inclination and 1 400 - 1 500 km altitude.

Considering the processing time, running a least squares for each candidate solution takes a long time. In this case, the calculation was performed on three processes in parallel with a total runtime of approximately 80 hours for each on a laptop with an Intel Core i56200U CPU with 2.30 GHz. The processing time of a single least squares is mainly dependent on the number of measurement points and the time between the two tracklets as this influences the computation time for the propagation.

Single Days - Medium LEO

As an additional test, four other days have been selected to run the correlation over the detections from 24 hours. Here, the dataset is limited to the objects in medium LEO to reduce the computation time, which is now approximately 20 hours per experiment, while still having a realistic chance for false positives due to objects in similar orbits. The results are summarised in Table 2. From nearly 10 million checked pairs, more than 1 000 true correlations are identified, which is approximately 80% if skipped pairs are excluded. The final correlations also contain nearly 20% false positives, but similar to the previous experiment those are mainly due to measured passes with a low number of detections.

Table 2: Results of single day correlation using medium LEO objects.

	Sample				Result		
Start Epoch	$N_{\text{tracklets}}$	N_{pairs}	N_{TP}	$N_{\text{TP,skipped}}$	N_{FN}	N_{TP}	N_{FP}
April 2, 12 UTC	1 990	1 979 055	472	104	69	299	97
April 3, 12 UTC	2 401	2 881 200	466	116	72	278	111
April 4, 12 UTC	1 983	1 965 153	283	70	43	170	15
April 5, 12 UTC	2 498	3 118 753	492	92	73	327	14
Total		9 944 161	1 713	382	257	1 074	237

Graph Analysis and Voting

The process of the graph analysis was introduced in (Reference 23) for optical measurements in GEO and it is extended here for the use with LEO radar data. Here, also the aspect of the correct determination of the number of revolutions is important because in the LEO case there may be multiple solutions leading to a correlation. As an example for this, Figure 18 shows two different true positive correlations and their Mahalanobis distances over the number of revolutions with an

assumed threshold of $M_\mathrm{d} = 5$. For the case of two detections being 35 revolutions apart, there is just one solution below the threshold, which is the correct one, but the more revolutions between the detections the shallower this minimum becomes because also the differences in semi-major axis between two adjacent solutions become smaller. For Figure 18a this difference is 130 km, whereas for Figure 18b it is only 14 km, which also leads to smaller variations in the orbital speed and thus range-rates. In total there are five solutions below the threshold for the case in Figure 18b. Especially for correlations with long time spans between the detections, it may be difficult to justify rejecting solutions which are not the minimum but still at a reasonable value. The large percentage of solutions with a wrong orbit as seen in the previous sections also shows that selecting the correct number of revolutions from a single pair of tracklets is very challenging.

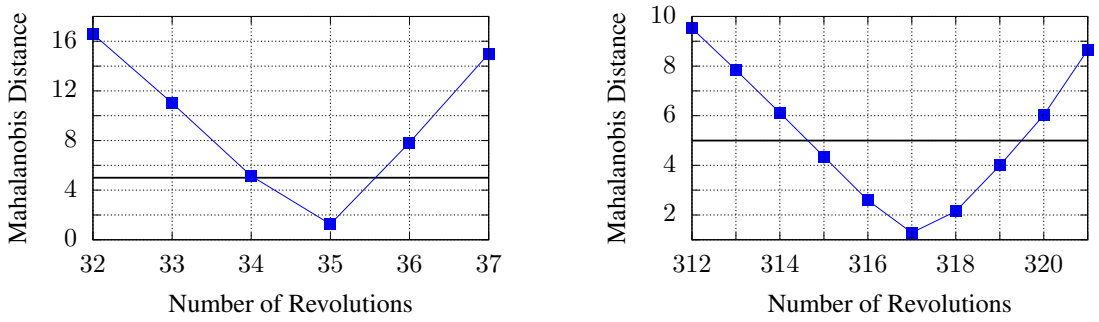

(a) 2.5 Days

(b) 22 Days

Figure 18: Two examples of the Mahalanobis distances over the numbers of revolutions (PFISR, medium LEO).

The applied principle is based on building a graph network with the tracklets as nodes which are connected by an edge if they are correlated, see also (Reference 24) for a similar approach. As a new addition, the graph network is now a so-called multigraph which means that it is possible to have multiple edges between the same pair of nodes. In the case here, an edge between two tracklets is created for each solution which can connect them with an acceptable orbit, i.e. passing both the M_d-threshold and the RPP. The orbit of this correlation is also attached to the edge as an additional information. As a next step, cycles in the graph consisting of three connected tracklets are formed. These groups are called triangles in the following, see (A,B,C) in Figure 19 as an example. While forming these triangles, an additional rule is enforced which checks if the three correlations in the triangle have a matching semi-major axis ($\Delta a < 2$ km) and inclination ($\Delta i < 0.85°$), because these orbital elements are assumed to remain roughly constant over several days at least. For highly perturbed orbits, e.g. due to drag, this condition would need to be reconsidered. The mean semi-major axis and inclination of the orbits from the correlations in the triangle are then added as an additional information to the triangle. The underlying idea is that solutions with a wrong number of revolutions are usually not consistent in their offset from the true semi-major axis as this is also dependent on the total number of revolutions, while the inclination serves as an additional constraint. Thus it is expected that only the true correlations lead to large clusters. The next step is to merge those triangles with a shared correlation, i.e. sharing two nodes, into a larger group, e.g. in Figure 19 the triangles (A,B,C), (A,B,D), (B,C,D) and (A,C,D) would be merged to form a final group of four tracklets if the involved triangles have a matching semi-major axis and inclination.

Due to the multiple edges, it is possible that a tracklet ends up in more than one group, but

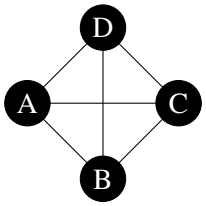

Figure 19: Example of a connected graph.

these groups are unconnected. In such a case, a majority vote will be used to decide the accepted group by selecting only the group with most tracklets. Because the process in the graph network is computationally very efficient compared to the least squares and increases its reliability with more available correlations, the threshold to add a correlation to the graph is set to $M_{\text{d,thresh}} = 10$ to maximise the number of candidate solutions for the following experiments. This approach can be applied to both the removal of false positives as well as the selection of the correct semi-major axis for a certain group.

Semi-major Axis Selection

As a first test, it is checked whether it is possible to select the correct semi-major axis from a group of tracklets. Two objects are chosen from the PFISR detections: Norad ID 32783 (28 tracklets) with [$a = 7008.769$ km, $e = 0.002$, $i = 98.04°$] and Norad ID 4719 (27 tracklets) with [$a = 7292.150$ km, $e = 0.013$, $i = 99.88°$]. Running the standard correlation with a hard selection of the semi-major axis leads to the percentages of wrong orbits as shown in Figure 20a. In total approximately 50% of the correlations have a wrong orbit. Processing now all candidate solutions, which passed both the $M_{\text{d,thresh}}$ and the RPP, with the described graph approach under consideration of the orbit leads to two groups with the correct orbit containing all of the corresponding object's tracklets. Thus the graph can be used to derive the correct solutions from all possible correlations.

To give an impression on the number of the considered solutions per correlation, Figure 20b depicts this number over the corresponding correlation's number of revolutions. As one would expect, the more revolutions the higher is the number of considered correlations with the majority reaching 5-15 correlations per pair for more than 100 revolutions and less than five before 50 revolutions.

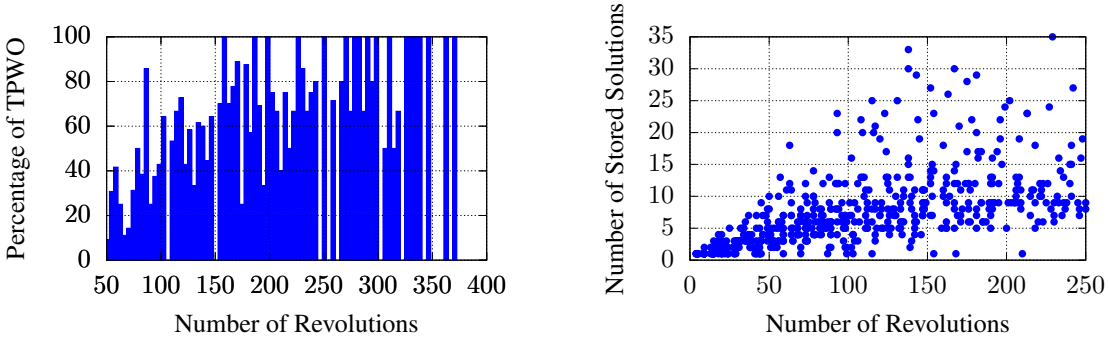

(a) Wrong orbit at minimum

(b) Number of considered solutions

Figure 20: Results comparing the percentage of the wrong orbits at the minimum $M_{\text{d,}}$. (left) to the number of solutions smaller than $M_{\text{d,thresh}}$.

Single Sensor - 5 Days

As a next step, the graph approach is tested in the presence of possible false positives. In order to have sufficient tracklets per objects, this test uses 1 500 PFISR tracklets from April 1, 12 UTC to April 6, 12 UTC of medium LEO objects. This leads to approximately 1.1 million total pairs to be checked including circa 2 600 true correlations. There are 277 objects with at least three tracklets, 186 with at least four tracklets, 116 with at least five tracklets and 57 with at least six tracklets.

Figure 21a gives an overview over the numbers of true and false positive correlations before and after the graph processing. Initially there are more than 10 000 false positives compared to approximately 2 000 true positives. After the analysis using the graph, the false positives are reduced to 21 correlations, while there is only a small reduction in true positives. To consider the number of identified objects instead of correlations, Figure 21b uses similar categories as for the correlations. TP-all designates an identified group which contains all and only tracklets from the same object, whereas a group with FN does not contain all tracklets of the object. The FP-group contains tracklets from different objects. Finally the missed groups are those objects with at least three tracklets that did not end up in an identified group. This is mainly the case when exactly three tracklets for one object are present and one of the correlations is missed, thus no triangle can be formed. In total, more than 80% of the objects are identified correctly, which also includes the selection of the correct semi-major axis and inclination. The FP-groups usually are not completely mixed with tracklets from different objects but they contain only one wrong tracklet among a group of true ones.

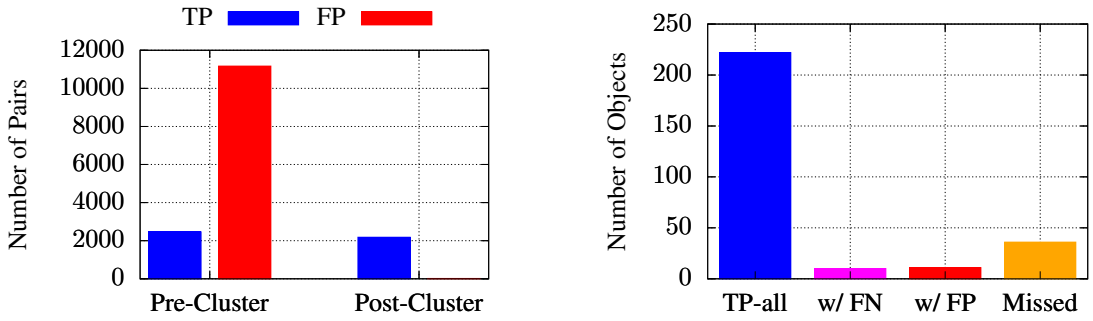

(a) True and wrong correlations

(b) Types of groups after clustering

Figure 21: Results of the correlation experiment (PFISR - 5 days) showing the true and false positive correlation (left) and the types of the identified groups.

In this case, the runtime is approximately 20 hours on three parallel processes for the creation of the candidate correlations. The graph analysis afterwards takes less than 10 seconds. Performing a least squares orbit determination for each of the candidate correlations instead would lead to a significant increase in processing time of tens of hours.

CONCLUSION

To sum up the results of the paper, it can be concluded that the correlation works well in general with real measurement data of the LeoLabs radars. This is also a confirmation of the usability of the correlation method, which had only been tested with simulated measurements before. This paper also introduced the application of a graph-based decision approach to identify objects and also to agree on its orbit by considering multiple possible solutions from the correlation. This approach has

the disadvantage that it requires at least three tracklets per object within the data, but if such objects are present they are likely to be identified. Comparing the processing times, the least squares takes a lot more time than performing the graph analysis but it has the advantage that it can also work on smaller datasets which reduces the number of possible combinations.

The analysis of the initial orbit determination and correlation also showed that the placement of the radar stations has a significant impact on the performance. Having a station at a low latitude like MSR allows it to have detections on different segments of the orbit, depending on its inclination, which improves the orbit determination in general. In contrast to that a high-latitude station like PFISR has a smaller spatial separation between detections on different segments of the orbit. However, it also has to be considered that the high-latitude stations have more visible passes for the densely populated polar orbits. With this in mind, the new LeoLabs station KSR in New Zealand should contribute very well to the existing set-up, especially in combination with PFISR considering correlation and orbit determination.

The use of the real data also confirmed many observations from previous work using simulated observations, e.g. the bias of the J_2-correction. This suggests that a reliable test of radar processing methods is possible by using realistic observation conditions when simulating data, such as e.g. range-dependent noise.

It is also important to note that the computational demands increase with more data, such that for large datasets provided continuously in a processing pipeline either sufficient computational resources have to be provided or special processing techniques could be employed to avoid testing all pairs of tracklets. One option for this could be to create the graph network of correlations in real-time, which would also allow it to have multiple hypotheses on the existence of objects until a confirmation criterion is met. Over time, the number of tracklets to be tested in the correlation framework would also decrease due to the build-up of a catalogue, because many observations could already be associated to a catalogue object. An automatic decision process for the confirmation of new objects as well as the associations between catalogue and observations are possible future research topics to extend the work presented here.

ACKNOWLEDGMENT

The first author is supported by the European Space Agency through the Networking/Partnering Initiative. The radar data was provided by LeoLabs under a contract with the European Space Agency.

REFERENCES

[1] J.-C. Liou and N. L. Johnson, "Risks in Space from Orbiting Debris," *Science*, Vol. 311, No. 5759, 2006, pp. 340–341, 10.1126/science.1121337.

[2] G. P. Fonder, P. J. Hack, and M. R. Hughes, "AN/FSY-3 Space Fence System–Sensor Site One/Operations Center Integration Status and Sensor Site Two Planned Capability," *Advanced Maui Optical and Space Surveillance (AMOS) Technologies Conference*, 2017.

[3] H. Wilden, C. Kirchner, O. Peters, N. Ben Bekhti, R. Kohlleppel, A. Brenner, and T. Eversberg, "GESTRA-technology aspects and mode design for space surveillance and tracking," *Proceedings of the 7th European Conference on Space Debris, Darmstadt, Germany*, 2017.

[4] I. McCrea, A. Aikio, L. Alfonsi, E. Belova, S. Buchert, M. Clilverd, N. Engler, B. Gustavsson, C. Heinselman, J. Kero, *et al.*, "The science case for the EISCAT_3D radar," *Progress in Earth and Planetary Science*, Vol. 2, No. 1, 2015, p. 21.

[5] R. Gomez, J. Martinez-Villa Salmeron, P. Besso, *et al.*, "Initial Operations of the Brealthrough Spanish Space Surveillance and Tracking Radar (S3TSR) in the European Context," *1st NEO and Debris Detection Conference*, 2019.

[6] K. Hill, C. Sabol, and K. T. Alfriend, "Comparison of covariance based track association approaches using simulated radar data," *The Journal of the Astronautical Sciences*, Vol. 59, No. 1-2, 2012, pp. 281–300.

[7] A. Vananti, T. Schildknecht, J. Siminski, B. Jilete, and T. Flohrer, "Tracklet-tracklet correlation method for radar and angle observations," *7th European Conference on Space Debris*, 4 2017. Presented paper.

[8] K. J. DeMars, I. I. Hussein, C. Frueh, M. K. Jah, and R. Scott Erwin, "Multiple-object space surveillance tracking using finite-set statistics," *Journal of Guidance, Control, and Dynamics*, Vol. 38, No. 9, 2015, pp. 1741–1756.

[9] E. Delande, J. Houssineau, J. Franco, C. Frueh, D. Clark, and M. Jah, "A new multi-target tracking algorithm for a large number of orbiting objects," *Advances in Space Research*, Vol. 64, No. 3, 2019, pp. 645–667.

[10] A. Milani, G. F. Gronchi, M. d. Vitturi, and Z. Knežević, "Orbit determination with very short arcs. I admissible regions," *Celestial Mechanics and Dynamical Astronomy*, Vol. 90, No. 1-2, 2004, pp. 57–85.

[11] J. M. Maruskin, D. J. Scheeres, and K. T. Alfriend, "Correlation of optical observations of objects in earth orbit," *Journal of Guidance, Control, and Dynamics*, Vol. 32, No. 1, 2009, pp. 194–209.

[12] K. J. DeMars, M. K. Jah, and P. W. Schumacher, "Initial orbit determination using short-arc angle and angle rate data," *IEEE Transactions on Aerospace and Electronic Systems*, Vol. 48, No. 3, 2012, pp. 2628–2637.

[13] K. Fujimoto, D. J. Scheeres, J. Herzog, and T. Schildknecht, "Association of optical tracklets from a geosynchronous belt survey via the direct Bayesian admissible region approach," *Advances in space research*, Vol. 53, No. 2, 2014, pp. 295–308.

[14] J. A. Siminski, O. Montenbruck, H. Fiedler, and T. Schildknecht, "Short-arc tracklet association for geostationary objects," *Advances in space research*, Vol. 53, No. 8, 2014, pp. 1184–1194.

[15] G. Tommei, A. Milani, and A. Rossi, "Orbit determination of space debris: admissible regions," *Celestial Mechanics and Dynamical Astronomy*, Vol. 97, No. 4, 2007, pp. 289–304.

[16] K. J. DeMars and M. K. Jah, "Probabilistic initial orbit determination using radar returns," *Proceedings of the AAS/AIAA Astrodynamics Specialist Conference (2013, Hilton Head, SC)*, Vol. 150, 2014, pp. 35–54.

[17] G. F. Gronchi, L. Dimare, D. Bracali Cioci, and H. Ma, "On the computation of preliminary orbits for Earth satellites with radar observations," *Monthly Notices of the Royal Astronomical Society*, Vol. 451, No. 2, 2015, pp. 1883–1891.

[18] B. Reihs, A. Vananti, and T. Schildknecht, "A Method for Perturbed Initial Orbit Determination and Correlation of Radar Measurements," *Advances in Space Research*, Vol. 66, No. 2, 2020, pp. 426 – 443, 10.1016/j.asr.2020.04.006.

[19] B. Reihs, A. Vananti, T. Schildknecht, J. Siminski, and T. Flohrer, "Application of Attributables to the Correlation of Surveillance Radar Measurements," *In Preparation*, 2020.

[20] P. Mahalanobis, "On the generalised distance in statistics," *Proceedings of the National Institute of Science of India*, Vol. 2, No. 1, 1936, pp. 49–55.

[21] M. Nicolls, V. Vittaldev, D. Ceperley, J. Creus-Costa, C. Foster, N. Griffith, E. Lu, J. Mason, I. Park, C. Rosner, *et al.*, "Conjunction Assessment for Commercial Satellite Constellations Using Commercial Radar Data Sources," *Advanced Maui Optical and Space Surveillance (AMOS) Technologies Conference*, 2017.

[22] N. Griffith, E. Lu, M. Nicolls, I. Park, and C. Rosner, "Commercial Space Tracking Services for Small Satellites," *Small Satellite Conference*, 2019.

[23] B. Reihs, A. Vananti, J. Siminski, T. Flohrer, and T. Schildknecht, "Analysing the Correlation Performance of ESAs Planned Space-based GEO Surveillance Mission," *70th International Astronautical Congress*, 10 2019.

[24] C. Yanez, J. C. Dolado Pérez, P. Richard, I. Llamas, and L. Lapasset, "Optical measurements association using optimized boundary value initial orbit determination coupled with Markov clustering algorithm," *7th European Conference on Space Debris*, 4 2017. Presented paper.